Quantum Electronics **31** (5) 448 – 452 (2001)

INTERACTION OF LASER RADIATION WITH MATTER. LASER PLASMA

PACS numbers: 52.50.Jm; 52.59.-f; 52.35.Qz
DOI: 10.1070/QE2001v031n05ABEH001976

Production of an extended plasma column in vacuum by irradiating a target by a quasi-Bessel beam

V M Batenin, S S Bychkov, L Ya Margolin, L N Pyatnitskii, A D Tal'virskii, E V Fomenko

***Abstract*. A technique of focusing the heating radiation was investigated, which makes it possible to produce an extended (under laboratory conditions, up to 1 m and over) plasma column and enables an easy output of VUV radiation. A plane solid-state target in vacuum was arranged along the caustic of a conic lens (axicon), which focused the laser beam. An analytic dependence, which describes the spatial intensity distribution of the heating radiation in the case of a nontransparent, partially reflecting target, was derived and experimentally verified. Experiments on the irradiation of an aluminium target in vacuum with a 5-J, 5-ns pulse of a neodymium-glass laser were performed. A plasma column up to 30 mm in length and no greater than 10 μm in diameter was formed. A rather intense plasma radiation was recorded in the VUV range.**

Keywords: *quasi-Bessel beam, laser plasma, plasma channel, VUV radiation.*

1. Introduction

High-power beams of laser radiation, in which the radial field amplitude distribution is described by the Bessel function and the longitudinal distribution is nearly constant, are unique instruments for the production of long (under laboratory conditions, up to 1 m and longer) continuous plasma channels in transparent media (gases and liquids) [1, 2].

Let us compare the extent of a Bessel beam of filamentary configuration (the radial distribution of the beam field is described by the zero-order Bessel function) produced when laser radiation is focused with a conic lens (axicon) with the lengths of the focal volumes of spherical and cylindrical lenses commonly used to produce extended plasma columns. When an input laser beam with a wavelength $\lambda \sim 1$ μm and radius $R \sim 2$ cm typical for laboratory experiments (the aperture of the focusing optics is assumed to be wider than R) is focused to a region with diameter, for instance, $d \sim 100$ μm, the length of this region L_{sp} is $\sim d^2/\lambda \sim 1$ cm when employing a spherical lens, $L_{cyl} \sim 2R \sim 4$ cm with a cylindrical lens, and $L_{con} \sim 2Rd/\lambda \sim 400$ cm with an axicon. Therefore, the extent of plasma columns with an axicon focusing of laser radiation may exceed those offered by spherical or cylindrical lenses by nearly two orders of magnitude.

The plasma columns produced upon the optical breakdown in a Bessel beam were used for the fast switching of electric signals [3] and the channelling of high-power laser pulses [4, 5]. These columns also show promise as the working medium of efficient lasers for the vacuum UV (VUV) and soft X-ray ranges [6 – 8]. One of the problems encountered in the realisation of this highly attractive application is the extraction of VUV radiation through the medium surrounding the plasma. This problem can be solved by isolating a gas target with the help of an intermediate volume with a differential pumping or by injecting a gas target in vacuum, but these methods are technically complicated.

In this paper, we tested a technique that makes it possible to produce an extended plasma column and enables an easy output of VUV radiation. A plane solid-state target in vacuum was arranged along the caustic of an axicon, which focused the laser beam. The use of a half the axicon aperture due to the target opacity resulted in moderate changes in the longitudinal and radial distributions of the heating radiation. The intensity of this quasi-Bessel beam in the focal region decreased by about a factor of two and still remained high enough to produce a hot plasma with an inverse population.

2. Characteristics of a quasi-Bessel beam

For an opaque target whose plane is arranged along the axicon caustic, a half the aperture of the focusing element contributes to the formation of the focal region. This scheme is unconventional and the intensity distribution of the heating radiation in the focal region was previously unknown. To determine this distribution, the heating field was theoretically analysed and special experiments were performed.

2.1 Analytical treatment

The field amplitude in the focal region away from its edges was written with the help of the Kirchhoff integral [9]. The integration was performed with respect to the azimuth angle φ and radius r in polar coordinates (the origin is located at the vertex of the axicon and the z axis is directed along its axis, the zero value of φ corresponds to the shadow boundary, and positive values of φ correspond to the open part of the axicon), similarly to the case of focusing with a totally open axicon (see, e. g., Ref. [10]). The diffe-

V M Batenin, S S Bychkov, L Ya Margolin, L N Pyatnitskii, A D Tal'virskii, E V Fomenko Institute of High Temperatures, Russian Academy of Sciences, Izhorskaya ul. 13/19, 127412 Moscow, Russia

Received 11 January 2001
Kvantovaya Elektronika **31** (5) 448 – 452 (2001)
Translated by E N Ragozin

rence is that the integration with respect to the angle φ between the initial value φ_0 and $\varphi_0 + 2\pi$ in Ref. [10] leads to a tabulated integral, while in our case it leads to a non-tabulated integral:

$$K(r, \varphi_0) = \int_0^{\pi} \exp[-\mathrm{i}x\cos(\varphi - \varphi_0)]\mathrm{d}\varphi, \quad (1)$$

where $x = kr\sin\gamma$; $k = 2\pi/\lambda$ is the modulus of the wave vector; λ is the wavelength of the heating radiation; and γ is the angle of beam inclination relative to the optical axis. We calculated the integral (1) by transforming it using the expansion of the function $\theta(\varphi)$, which is defined as

$$\theta(\varphi) = \begin{cases} 1 & \text{for} \quad 0 \leqslant \varphi \leqslant \pi, \\ 0 & \text{for} \quad \pi < \varphi < 2\pi, \end{cases} \quad (2)$$

to a series of the sines of arguments with odd coefficients. The integration of expression (1), using tabulated integrals containing trigonometric functions of trigonometric functions, yielded the result:

$$K(r, \varphi_0) = \int_0^{2\pi} \exp[-\mathrm{i}x\cos(\varphi - \varphi_0)] \times \left[\frac{1}{2} + \frac{2}{\pi}\sum_{n=0}^{\infty}\frac{\sin(2n+1)\varphi}{2n+1}\right]\mathrm{d}\varphi$$

$$= \pi J_0(x) - 4\mathrm{i}\sum_{n=0}^{\infty}(-1)^n\frac{\sin(2n+1)\varphi_0}{2n+1}J_{2n+1}(x). \quad (3)$$

Finally, the expression for the intensity I_B of the Bessel beam produced when a plane wave of intensity I_in was focused with an axicon [2],

$$I_\mathrm{B}(z, r) = I_\mathrm{in}kz\sin^2\gamma 2\pi J_0^2(kr\sin\gamma), \quad (4)$$

assumed the following form when the focusing was accomplished with a half-closed axicon:

$$I_\mathrm{qB}(z, r, \varphi) = I_\mathrm{in}kz\sin^2\gamma\left\{\frac{\pi}{2}J_0^2(kr\sin\gamma) + \frac{8}{\pi}\left[\sum_{n=0}^{\infty}(-1)^n\frac{\sin(2n+1)\varphi}{2n+1}J_{2n+1}(kr\sin\gamma)\right]^2\right\}. \quad (5)$$

Strictly speaking, the intensity distribution in the case of a plane target arranged along the caustic is not completely similar to that produced with a half-closed axicon. One of the reasons for this difference is the reflection from the target and the interference of the incident radiation with the mirror part of the reflected radiation. If the phase change in the reflection is neglected, the presence of the reflected radiation is equivalent to a partial transparency of the screen closing one-half the axicon aperture. In this case, the distribution (5) for a quasi-Bessel beam is transformed as:

$$I_\mathrm{qB}(z, r, \varphi) = I_\mathrm{in}kz\sin^2\gamma\left\{\frac{\pi(1+\sqrt{g})^2}{2}J_0^2(kr\sin\gamma) + \frac{8(1-\sqrt{g})^2}{\pi}\left[\sum_{n=0}^{\infty}(-1)^n\frac{\sin(2n+1)\varphi}{2n+1}J_{2n+1}(kr\sin\gamma)\right]^2\right\}, \quad (6)$$

where g is the reflection coefficient.

Therefore, the intensity distribution of interest to us exhibits the dependence on the azimuthal angle. An analysis of expressions (5) and (6) shows that this dependence is symmetric about the shadow boundary $[I_\mathrm{qB}(-\varphi) = I_\mathrm{qB}(\varphi)]$ and about the direction perpendicular to the boundary $[I_\mathrm{qB}(\pi/2 - \varphi) = I_\mathrm{qB}(\pi/2 + \varphi)]$. In particular, along the shadow boundary ($\varphi = 0$ and π), we have

$$I_\mathrm{qB}(r, 0) = I_\mathrm{qB}(r, \pi) = I_\mathrm{in}kz\sin^2\gamma\,\frac{\pi(1+\sqrt{g})^2}{2}J_0^2(kr\sin\gamma). \quad (7)$$

For the direction perpendicular to the boundary ($\varphi = \pi/2$), we obtain

$$I_\mathrm{qB}\left(r, \frac{\pi}{2}\right) = I_\mathrm{in}kz\sin^2\gamma\left\{\frac{\pi(1+\sqrt{g})^2}{2}J_0^2(kr\sin\gamma) + \frac{8(1-\sqrt{g})^2}{\pi}\left[\sum_{n=0}^{\infty}\frac{1}{2n+1}J_{2n+1}(kr\sin\gamma)\right]^2\right\}. \quad (8)$$

The half-tone patterns corresponding to expression (6) and dependences (7) and (8) are shown in Fig. 1 for $g = 0$, 0.03, and 0.3. The intensity distribution in the cross section of the focal region is invariant to shifts along the beam axis (to variation of z).

An analysis of the amplitudes of the terms of the infinite sums in expressions (6) and (8) reveals that the main contribution to the intensity is made by the first terms of the sums. For instance, summing up to $n = 2$ provides an error of the order of 10 % in the intensity determination. The fact that the resultant field distribution can be represented as a combination of several Bessel functions and its invariance to changes in z give grounds to refer to the beam with an intensity distribution described by expression (6) as a quasi-Bessel one.

2.2 Model experiments

We studied experimentally the intensity distribution in the cross section of the focal region of the axicon, with its aperture partially shielded and the intensity distribution at the target positioned along the beam axis. The scheme of measurements in the cross section is shown in Fig. 2. The beam of He–Ne laser (*1*) radiation ($\lambda \sim 0.63$ μm) attenuated with an optical filter (*2*) was expanded with a collimator (*3*) up to 15 mm in diameter limited by an aperture (*4*) and was focused by an axicon (*6*). An axicon with a small base angle $\alpha \sim 2^\circ$ was used. Because of a relatively large caustic diameter d ($d \sim \lambda/\gamma \sim 40$ μm, $\gamma \sim 0.5\alpha$), the requirements on the measurement accuracy were not very strict.

A part of the axicon aperture bounded by a chord was shielded with a mask (*5*) (h is the height of the shielded segment). Particular attention was given to the measurements where a half of the aperture was shielded; also investigated were the cases of intermediate mask positions. The intensity distribution in the cross section of the caustic (*9*) was projected with an objective (*7*) with a mag-nification $\beta \sim 6^\times$ on the CCD array of a digital camera (*8*). The images obtained at different distances from the axicon were virtually similar, differing only in intensity.

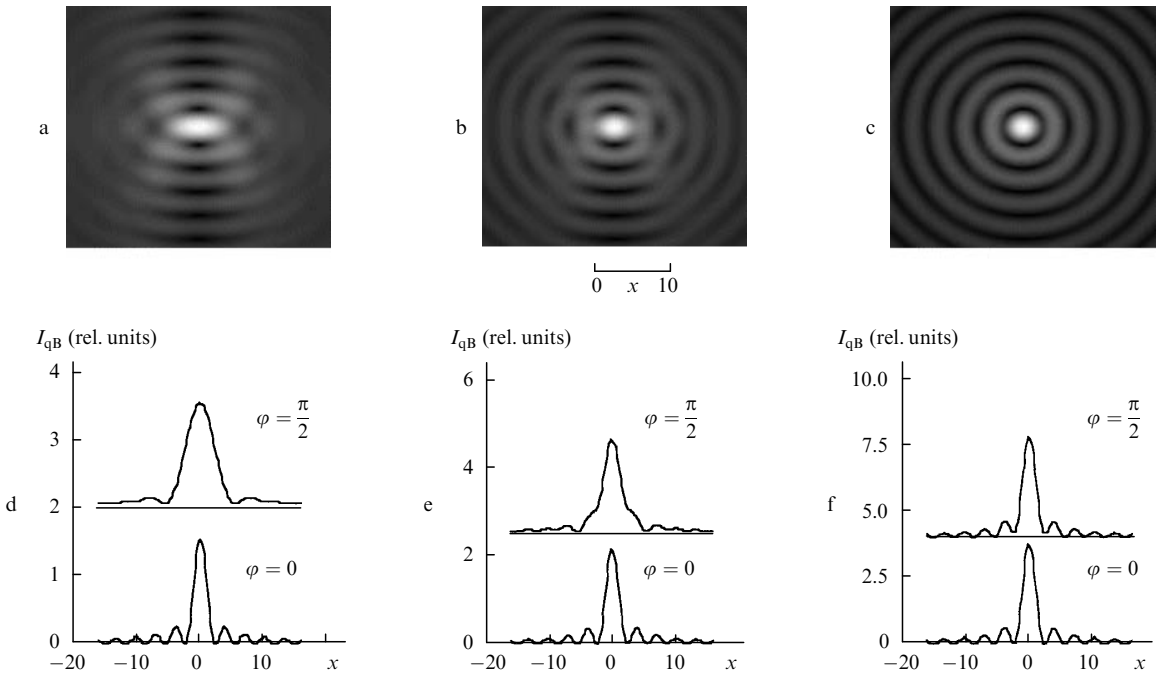

Figure 1. Half-tone intensity distribution patterns $I_{qB}(x, \varphi)$ in the cross section of the quasi-Bessel beam (a–c) and corresponding dependences $I_{qB}(x)$ for the paths directed along ($\varphi = 0$) and across ($\varphi = \pi/2$) the shadow boundary (d–f) for the reflection coefficient $g = 0$ (a, d), 0.03 (b, e), and 0.3 (c, f).

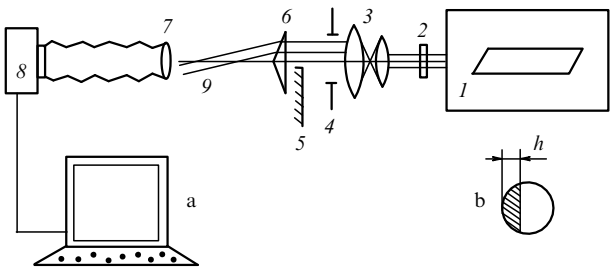

Figure 2. Schematic of the measurements of intensity distribution in the cross section of the quasi-Bessel beam (a) and the cross section of a partially shielded aperture (b) (see text).

Fig. 3 shows typical examples of the distributions obtained for a full-aperture axicon (Fig. 3a) and a half-shielded axicon (Fig. 3b). The corresponding axicon apertures are shown schematically at the top left of the half-tone pictures. A comparison of these results with the calculated data obtained above indicates that they agree closely with each other. Small changes in h ($\Delta h \sim 25d$) resulted in insignificant changes in the intensity distribution (Fig. 3c,d).

An analysis of the distributions obtained shows that the intensity distribution along the direction of the shadow boundary is adequately described by the square of the Bessel function both with a half-shielded axicon aperture ($h = R$, where R is the axicon radius) and without shielding, the diameters of the corresponding peaks in this case remaining invariable. The intensity distribution in the direction perpendicular to the shadow boundary is also close to the square of the Bessel function, but the diameters of the corresponding peaks increase by a factor of ~ 2.

As the fraction of the shielded axicon aperture increased ($R < h < 2R$), the intensity distribution pattern lengthened in the direction perpendicular to the shadow boundary, but almost did not change in the direction parallel to the boundary. While for $h = R$ the width of the principal peak increased by a factor of ~ 2, for $h = 1.5R$ the increase was approximately three-fold, and for $h \sim 2R$ nearly five-fold. The total energy contained in the principal peak varied nearly in proportion to the area of the open axicon aperture. In particular, shielding one-half the axicon aperture decreased the energy by a factor of ~ 2.2.

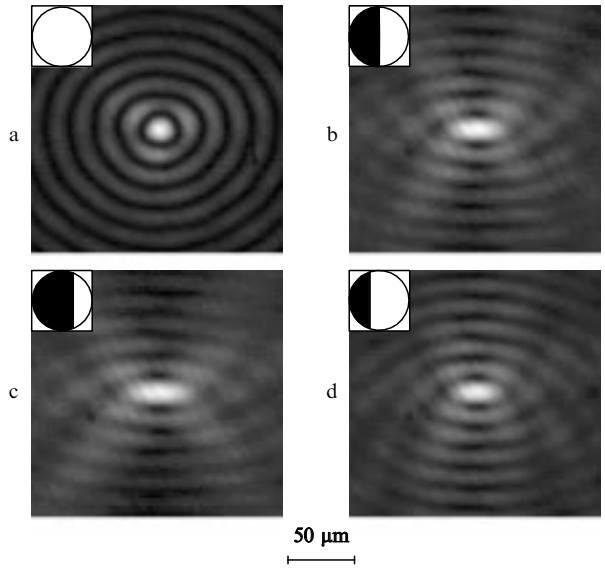

Figure 3. Intensity distributions obtained for an open axicon (a), a half-shielded axicon ($\Delta h = 0$, b), and an axicon with more ($\Delta h \simeq 25d$, c) and less ($\Delta h \simeq -25d$, d) than one-half the aperture shielded.

The arrangement was slightly changed to measure the distribution at the target positioned along the beam axis: the mask was absent, a plane opaque target was placed in the caustic, and the measuring device was accordingly rotated. The resultant image consisted of a bright principal streak along the axis of the focal region and additional streaks of lower intensity. The steak widths and their separations corresponded to the radiation intensity distribution behind the open axicon.

Consider the potentialities of a quasi-Bessel beam irradiating a target to produce hot plasmas. The typical intensities I of the heating radiation at hand lie in the $\sim 10^{11} - 10^{12}$ W cm^{-2} range [11]. Under these intensities, the electron temperature in the plume produced by exposing a target to 1.06-μm radiation can be estimated with the aid of the scaling of Ref. [12], assuming a ratio between the atomic mass and the average charge $\langle A\rangle/\langle Z\rangle \sim 4 - 10$ for plasma ions:

$$T_e \simeq 2.7\ \text{keV}\left(\frac{I}{10^{14}\ \text{W cm}^{-2}}\right)^{2/3}\left(\frac{\lambda}{1\ \mu\text{m}}\right)^{4/3}\left(\frac{\langle A\rangle}{2\langle Z\rangle}\right)^{1/3}$$

$$\sim 50 - 200\,\text{eV},$$

which is sufficient for producing a plasma with inverse population [13].

Therefore, the plume produced by a quasi-Bessel beam at the target can be considered as a potential working medium of an X-ray laser.

3. Experimental

We performed special experiments to verify the realisability of the proposed technique of formation of a hot plasma. We used the heating radiation of neodymium-glass laser (5 J, 5 ns) focused with a glass axicon with a base angle $\alpha = 30^\circ$ or 20° on a plane aluminium target (a 0.02-mm thick foil or a 5-mm thick plate) in vacuum. The exterior view of the plasma column and the emission spectra in the visible and VUV ranges were recorded.

The measurement scheme is shown in Fig. 4. The radiation of a laser (*1*) was focused by an axicon (*2*) on a target (*3*) located in the vacuum chamber (*4*). The emission spectra of a plasma in the lateral and axial directions were analysed and recorded respectively by a DFS-452 diffraction spectrograph (*5*) coupled to a digital video camera (*6*) (the visible range) and a grazing-incidence VUV spectrograph (*7*) on UF-4 photographic film (the VUV range). A quartz lens (*8*) was used to project a 2.2 times demagnified image of a fragment of the plasma channel across the entrance slit of the DFS-452 spectrograph. The side view of the same fragment in the visible range six times magnified with an objective (*9*) was recorded with a digital video camera (*10*). A selected combination of optical filters (*11*) ensured recording the images in the linear response region of the CCD array. When a foil target was used, two similar plasma channels were produced on both sides of the target, and therefore the spectrum in the visible range and the exterior view of the plasma were recorded simultaneously. With a massive target, the above images were recorded during different laser shots.

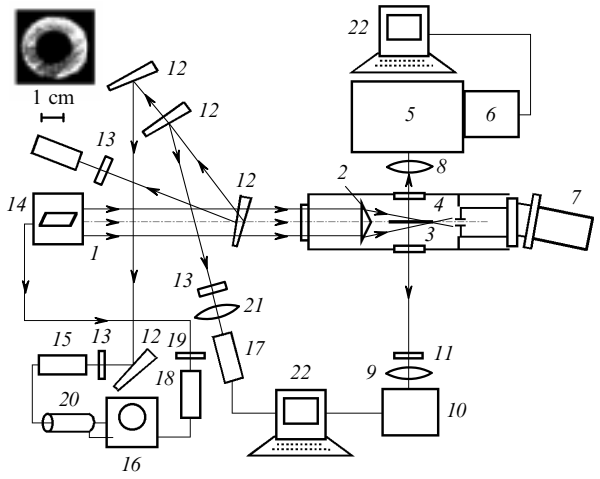

Figure 4. Schematic of the experiment to generate a plasma channel on a target in vacuum (see text).

We used in the experiments a single-mode pulsed neodymium-glass laser with a telescopic amplifier ($\lambda = 1.054$ μm). The energy in a 5-ns pulse amounted to 5 J, the beam divergence was $\sim 3 \times 10^{-4}$ rad. To measure the pulse energy, the temporal pulse shape, and the spatial intensity distribution in the laser beam, the radiation was split with wedges (*12*), attenuated with filters (*13*), and recorded respectively by a calorimeter (*14*), a coaxial photo-cell (*15*) coupled to a wide-band oscilloscope (*16*), and a digital video camera (*17*). The oscilloscope was triggered with the aid of the second coaxial photocell (*18*). The amplitude of the triggering pulse was selected by optical filters (*19*) and the instant of recording, by a delay line (*20*). The image of the cross section of the laser beam was transferred from the plane optically conjugated with the axicon to the CCD array with the help of objective (*21*). An example of the typical radiation intensity distribution in front of the axicon is presented at the top left of the schematic in the form of a half-tone pattern. The obtained data were stored and processed by two PCs (*22*).

4. Results of measurement

The emission region of the produced plasma represented a thin bright streak up to 35 mm long and ~ 100 μm wide. The brightness was maximal in the paraxial region and decreased gradually toward the periphery with radius and toward the edges with distance. The emission brightness with a longitudinal scale length of ~ 150 μm was modulated in the axial direction. For an oblique incidence of the heating radiation on the target, the existence of such a modulation and its scale length are consistent with the known existence and scale length of the ordered structures in a laser-produced plasma plume [12]. A typical fragment of the image is shown in Fig. 5a. For comparison, Fig. 5b shows a fragment of the image of a spark channel produced in a gas target (argon, 1 bar) for the same conditions. The comparison shows that both plasma columns have close characteristic dimensions.

Fig. 5c shows a fragment of the trace of the plasma column on the target observed with a microscope after irradiation by several heating pulses. One can discern the boundaries of two regions: a narrow streak ~ 6 μm in width and a broader streak ~ 60 μm in width. The first region is likely to result from the action of intense radiation and (or) the produced hot dense plasma, while the second one can be

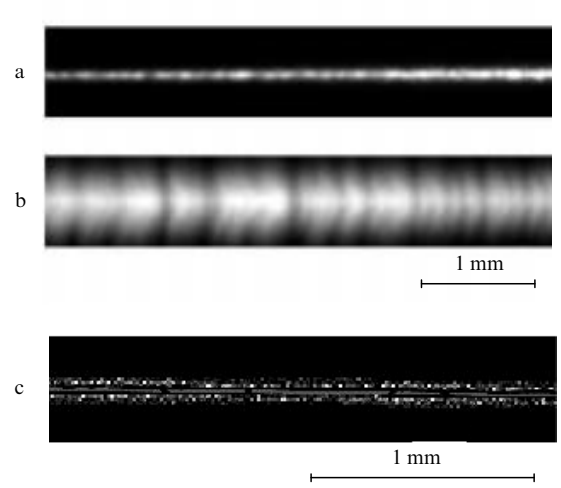

Figure 5. Fragments of the images of the plasma channel on a target in vacuum (a), the spark channel in argon (b), and the trace on the target (c).

produced by the action of the expanding lower-temperature plasma. Therefore, the trace on the target confirms the emergence of an extended plasma channel ~ 10 μm in diameter.

Fig. 6 shows fragments of the plasma emission spectra in the visible and VUV ranges with aluminium ion lines. The 559.3-nm line of Al II (15.4 eV), the 569.6-nm and 572.3-nm lines of Al III (17.81 and 17.80 eV) were observed in the visible region. An analysis of the VUV spectra revealed the presence of the emission lines of multiply charged aluminium ions: 13.0, 16.0, and 16.2 nm (95, 77, and 77 eV) of Al IV; 12.6, 13.0, and 28.0 nm (99, 95, and 44 eV) of Al V.

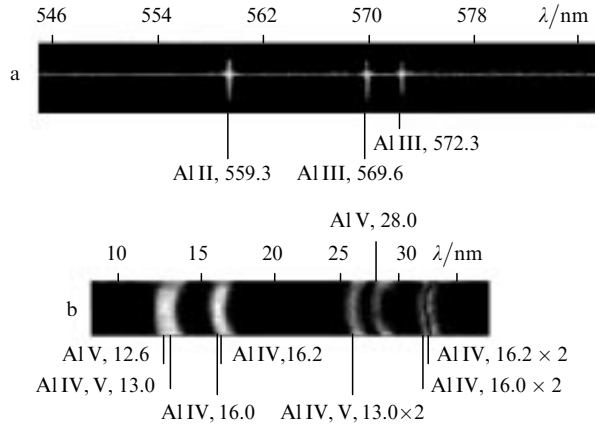

Figure 6. Fragments of the emission spectra of a plasma channel on a target in the visible (a) and VUV (b) ranges (the line wavelengths are given in nanometres; ×2 denotes the second diffraction order).

The presence of VUV lines of appreciable intensity in the plasma emission confirms that the electron temperature is high. Combined with the ease of increasing the plume length and the possibility to extract the VUV radiation, this circumstance allows us to consider the plume at a solid-state target in a quasi-Bessel beam as a promising medium for a VUV laser.

Acknowledgements. The authors are grateful to S V Gorlov, L M Maiorov, and A V Makarov for their assistance in performing the experiments. This work was supported in part by the Russian Foundation for Basic Research (Grant No. 99-02-16007) and the 'Integration' Federal Dedicated Programme (Grant No. A-0111).

References

1. Bunkin F V, Korobkin V V, Kurinyi Yu A, Polonskii L Ya, Pyatnitskii L N *Kvantovaya Elektron.* **10** 443 (1983) [*Sov. J. Quantum Electron.* **13** 254 (1983)]
2. Andreev N E, Margolin L Ya, Pleshanov I V, Pyatnitskii L N *Zh. Eksp. Teor. Fiz.* **105** 1232 (1994)
3. Marin M Yu, Pil'skii V I, Polonskii L Ya, Pyatnitskii L N, Reingol'd A V *Zh. Tekh. Fiz.* **75** 1507 (1987); Polonskiy L Ya, Goltsov A Yu, Morozov A V *Phys. Plasmas* **3** 2781 (1996)
4. Durfee C G, Lynch J, Milchberg H M *Phys. Rev. E: Stat. Phys., Plasmas, Fluids, Relat. Interdiscip. Top.* **51** 2368 (1995)
5. Nikitin S P, Alexeev I, Fan J, Milchberg H M *Phys. Rev. E: Stat. Phys., Plasmas, Fluids, Relat. Interdiscip. Top.* **59** R3839 (1999)
6. Bychkov S, Marin M, Pyatnitsky L *Proceedings of the Third International Colloquium on X-ray Lasers* (Schliersee, Germany, 1992) p. 439
7. Milchberg H M, Durfee C G, Lynch J *J. Opt. Soc. Am. B: Opt. Phys.* **12** 731 (1995); Milchberg H M, Durfee C G, McIlrath T J *Phys. Rev. Lett.* **75** 2494 (1995)
8. Muendel M H, Fluery M, Chatterji S K, Demeris T, Geuthier J-C, Hagelstein P L *X-ray Lasers 1996 (Proceedings of the Fifth International Conference on X-ray Lasers, Lund, Sweden, 1996)* S Svanberg, C-G Wahlstrom (Eds) (Bristol: IOP Publishing, 1996) p. 301
9. Born M, Wolf E *Principles of Optics* (Oxford: Pergamon Press, 1969)
10. Korobkin V V, Polonskii L Ya, Poponin V P, Pyatnitskii L N *Kvantovaya Elektron.* **13** 265 (1986) [*Sov. J. Quantum Electron.* **16** 178 (1986)]
11. Bychkov S S, Gorlov S V, Margolin L Ya, Pyatnitskii L N, Tal'virskii A D, Shpatakovskaya G V *Kvantovaya Elektron.* **26** 229 (1999) [*Quantum Electron.* **29** 229 (1999)]
12. Koroteev N I, Shumai I L *Fizika Moshchnogo Lazernogo Izlucheniya* (The Physics of High-Power Laser Radiation) (Moscow: Nauka: 1991) p. 174
13. Elton R *X-ray Lasers* (New York: Academic Press, 1990) p. 90